Fluid and Plasmadynamics Conference, report no. 77–682, 27–29 June (1977).
10. A. P. Hatton and P. J. Walklate, A mixing-length method for predicting heat transfer in rough pipes, *Int. J. Heat Mass Transfer* **19**, 1425–1431 (1976).
11. A. T. Wassel and A. F. Mills, Calculation of variable property turbulent friction and heat transfer in rough pipes (to be submitted for publication) (1981).
12. J. A. Schetz and B. Nerney. Turbulent boundary layer with injection and surface roughness, *AIAA Jl* **15**, 1288–1294 (1977).
13. J. M. Healzer, R. J. Moffat and W. M. Kays, The turbulent boundary layer on a rough, porous plate: experimental heat transfer with uniform blowing, report no. HMT-18, Thermosci. Div., Dept. of Mech. Engineering, Stanford University (1974).
14. P. M. Ligrani, R. J. Moffat and W. M. Kays, The thermal and hydrodynamic behavior of thick, rough-wall turbulent boundary layers, report no. HMT-29, Thermosci. Div., Dept. of Mechanical Engineering, Stanford University (1979).
15. D. F. Dipprey and R. Sabersky, Heat and momentum transfer in smooth and rough tubes at various Prandtl numbers, *Int. J. Heat Mass Transfer* **6**, 329–353 (1963).
16. M. E. Crawford and W. M. Kays, STAN5—A program for numerical computation of two-dimensional internal/external boundary layer flows, report No. HMT-23, Thermosci. Div., Dept of Mechanical Engineering, Stanford University (1975).
17. J. Nikuradse, Strömungsgesetze in rauhen Rohren, VDI Forschungsschaft, No. 361 (1933). English translation, NACA-TM 1292 (1950).
18. M. M. Pimenta, R. J. Moffat and W. M. Kays, The turbulent boundary layer: an experimental study of the transport of momentum and heat with the effect of roughness, report No. HMT-21, Thermosci. Div., Dept of Mechanical Engineering, Stanford University (1975).
19. H. W. Coleman, R. J. Moffat and W. M. Kays, Momentum and energy transport in the accelerated fully rough turbulent boundary layer, report No. HMT-24, Thermosci. Div., Dept of Mechanical Engineering, Stanford University (1976).

Int. J. Heat Mass Transfer. Vol. 24, No. 4, pp. 778–781, 1981
Printed in Great Britain

0017-9310/81/040778-04 $02.00/0

A NUMERICAL METHOD FOR THE SOLIDIFICATION OF A BINARY ALLOY

GUNTER H. MEYER
School of Mathematics, Georgia Institute of Technology, Atlanta, GA 30332, U.S.A.

(*Received* 6 *May* 1980 *and in revised form* 20 *October* 1980)

NOMENCLATURE

c, normalized concentration;
$\hat{c}$, heat capacity, $[J\,°C\,kg^{-1}]$;
D, mass diffusivity, $[m^2\,s^{-1}]$;
k, thermal conductivity, $[J\,°C\,m^{-1}\,s^{-1}]$;
L, length of slab, [m];
R, defined by equation (11);
r, mass flux, Dc';
S, defined by equation (12);
s, location of the phase front;
t, time variable, [s];
u, temperature, [°C];
u^*, interface temperature, [°C];
v, heat flux, ku';
w, defined by equation (13);
x, length variable, [m];
z, defined by equation (14).

Greek symbols

α, boundary temperature, [°C];
β, boundary concentration;
Δt, time step, [s];
λ, heat of fusion, $[J\,kg^{-1}]$;
ρ, mass density, $[kg\,m^{-3}]$.

Subscripts

$+$, indicates liquid phase;
$-$, indicates solid phase;
0, indicates initial time;
$n-1$, indicates time level $n-1$.

Superscripts

$'$, d/dx.

1. INTRODUCTION

IT IS the purpose of this communication to introduce a numerical method for the solidification of a one-dimensional binary alloy. The method is a straightforward extension of the technique described in [4] for the two-phase Stefan problem. It is applied to the heat and mass balance equations and specifically tracks the phase front. The method has several useful features:

(1) It applies to the primary variables of temperature and solute concentration.
(2) It permits solute diffusion both in the liquid and solid phase.
(3) General phase diagrams are acceptable for the liquid–solid phase change.
(4) The method is applicable to systems with heat and concentration dependent diffusion parameters.
(5) The method is time implicit and can cope with discontinuous systems as well as with the vastly different time constants for the heat and mass diffusion. Last, but not least the method is straightforward to implement and cheap to run.

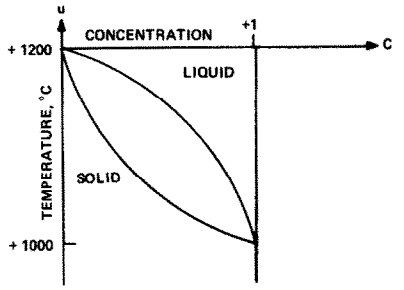

FIG. 1. Phase diagram for a binary alloy. Liquidus: Parabola through (0, 1200), (0.7, 1100), (1, 1000); solidus: Parabola through (0, 1200), (0.3, 1100), (1, 1000).

2. MODEL AND ALGORITHM

We shall use the model recently discussed in [2] for heat and mass transport in the liquid over the interval $[0, s(t)]$ (indexed with the subscript $+$), in the solid over the interval $[s(t), L]$ (indexed with $-$) and across the interface $x = s(t)$

Heat transport

$$\frac{\partial}{\partial x}\left(k_{\pm}\frac{\partial u_{\pm}}{\partial x}\right) - (\hat{c}\rho)_{\pm}\frac{\partial u_{\pm}}{\partial t} = 0. \tag{1}$$

Mass transport

$$\frac{\partial}{\partial x}\left(D_{\pm}\frac{\partial c_{\pm}}{\partial x}\right) - \frac{\partial c_{\pm}}{\partial t} = 0. \tag{2}$$

Continuity of temperature on the interface

$$u_{+} = u_{-} = u^{*} \tag{3}$$

where u^{*} is an unknown function of time and space.

Energy balance on the interface

$$\lambda\rho\frac{\mathrm{d}s}{\mathrm{d}t} - k_{-}\frac{\partial u_{-}}{\partial x} + k_{+}\frac{\partial u_{+}}{\partial x} = 0. \tag{4}$$

Mass balance on the interface

$$[c_{+} - c_{-}]\frac{\mathrm{d}s}{\mathrm{d}t} - D_{-}\frac{\partial c_{-}}{\partial x} + D_{+}\frac{\partial c_{+}}{\partial x} = 0. \tag{5}$$

In contrast to the linear relationship employed in [2] we shall link the interface concentrations and temperature through a general phase relationship for a binary mixture

$$c_{\pm} = g_{\pm}(u^{*}). \tag{6}$$

A typical phase diagram is shown in Fig. 1. (We remark that for some eutectics the condition (6) must be replaced by its inverse relation $u^{*} = \tilde{g}_{\pm}(c_{\pm})$; our method remains applicable in principle but its implementation will depend strongly on the form of the functions $\tilde{g}_{\pm}$.)

The boundary data are written as $u_{+}(0, t) = \alpha_{+}(t), u_{-}(L, t) = \alpha_{-}(t), c_{+}(0, t) = \beta_{+}(t)$ and $c_{-}(L, t) = \beta_{-}(t)$. Flux data can be handled as well but would require a modification of the existing computer program. Initial data are assumed given as $u_{\pm}(x, 0) = u_{0}(x)$, $c_{\pm}(x, 0) = c_{0}(x)$, $s(0) = s_{0}$. The initial/boundary data need not be continuous.

For the numerical solution these equations are time discretized and converted to first order systems. Assuming that we have the temperature u_{n-1}, the concentration c_{n-1} and the interface s_{n-1} at time t_{n-1} we obtain the new solution at $t_{n} = t_{n-1} + \Delta t$ from

$$u'_{\pm} = \frac{1}{k_{\pm}}v_{\pm} \qquad c'_{\pm} = \frac{1}{D_{\pm}}r_{\pm}$$

$$v'_{\pm} = \frac{(\hat{c}\rho)_{\pm}}{\Delta t}[u_{\pm} - u_{n-1}(x)] \quad r'_{\pm} = \frac{1}{\Delta t}[c_{\pm} - c_{n-1}(x)]$$

subject to $u_{+}(0) = \alpha_{+}(t_{n}), u_{-}(L) = \alpha_{-}(t_{n}), c_{+}(0) = \beta_{+}(t_{n}), c_{-}(L) = \beta_{-}(t_{n})$. The interface is determined from

$$\lambda\rho\frac{s - s_{n-1}}{\Delta t} - v_{-}(s) + v_{+}(s) = 0 \tag{7}$$

$$[c_{+} - c_{-}]\frac{s - s_{n-1}}{\Delta t} - r_{-}(s) + r_{+}(s) = 0 \tag{8}$$

where $c_{\pm} = g_{\pm}(u^{*})$ and $u^{*} = u_{+}(s) = u_{-}(s)$.

It is well known [4] that the temperature and concentration are related to their fluxes through the Riccati transformations

$$u_{\pm}(x) = R_{\pm}(x)v_{\pm}(x) + w_{\pm}(x) \tag{9}$$

$$c_{\pm}(x) = S_{\pm}(x)r_{\pm}(x) + z_{\pm}(x) \tag{10}$$

where $R_{\pm}$ and $S_{\pm}$ are the solutions of

$$R'_{\pm} = \frac{1}{k_{\pm}} - \left(\frac{\hat{c}\rho}{\Delta t}\right)_{\pm}R_{\pm}^{2} \tag{11}$$

$$S'_{\pm} = \frac{1}{D_{\pm}} - \frac{1}{\Delta t}S_{\pm}^{2} \tag{12}$$

subject to $R_{+}(0) = 0, R_{-}(L) = 0, S_{+}(0) = 0, S_{-}(L) = 0$, while $w_{\pm}$ and $z_{\pm}$ satisfy the initial value problems

$$w'_{\pm} = -\left(\frac{\hat{c}\rho}{\Delta t}R(x)\right)_{\pm}(w_{\pm} - u_{n-1}(x))$$

$$w_{+}(0) = \alpha_{+}(t_{n}), w_{-}(L) = \alpha_{-}(t_{n}) \tag{13}$$

$$z'_{\pm} = -\left(\frac{S(x)}{\Delta t}\right)_{\pm}(z_{\pm} - c_{n-1}(x))$$

$$z_{+}(0) = \beta_{+}(t_{n}), z_{-}(L) = \beta_{-}(t_{n}). \tag{14}$$

The solutions of equations (11)–(14) may be assumed known over $[0, L]$, sometimes analytically if the coefficients are constant, or numerically. The interface s_{n} is then determined as follows. If the interface is at the arbitrary point x then it follows from (9) that the heat fluxes are given by

$$v_{\pm} = \frac{u^{*} - w_{\pm}(x)}{R_{\pm}(x)}$$

where u^{*} is as yet undetermined. Substitution into (7) shows that u^{*} must satisfy

$$u^{*}(x) = \left[\lambda\rho\frac{x - s_{n-1}}{\Delta t} + \frac{w_{-}(x)}{R_{-}(x)} - \frac{w_{+}(x)}{R_{+}(x)}\right] \Bigg/ \left(\frac{1}{R_{-}(x)} - \frac{1}{R_{+}(x)}\right). \tag{15}$$

The interface s is found if for $x = s$ the equation (8) can be satisfied. Since

$$r_{\pm}(x) = \frac{c_{\pm}(x) - z_{\pm}(x)}{S_{\pm}(x)}$$

and $c_{\pm}(x) = g_{\pm}(u^{*})$ this amounts to searching for a root of the equation

$$\phi(x) = [g_{+}(u^{*}) - g_{-}(u^{*})]\left(\frac{x - s_{n-1}}{\Delta t}\right) - \frac{g_{-}(u^{*}) - z_{-}(x)}{S_{-}(x)} + \frac{g_{+}(u^{*}) - z_{+}(x)}{S_{+}(x)} = 0 \tag{16}$$

where u^{*} is given by equation (15).

Only those roots s_{n} of $\phi(x) = 0$ are meaningful for which $u^{*}(s_{n})$ lies in the phase change region indicated by the phase diagram. In our numerical work only one root was found in

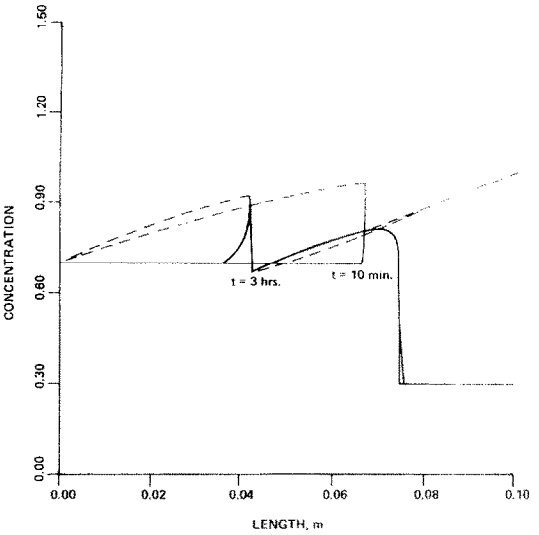

FIG. 2. Concentration in the slab after 10 min and after 3 h. Solid lines: computed concentrations. Broken lines: maximum permissible concentrations for the computed temperatures. 1400 space mesh points, 630 time steps increasing from 2 s to 2 min; Cyber 74 execution time 5 min.

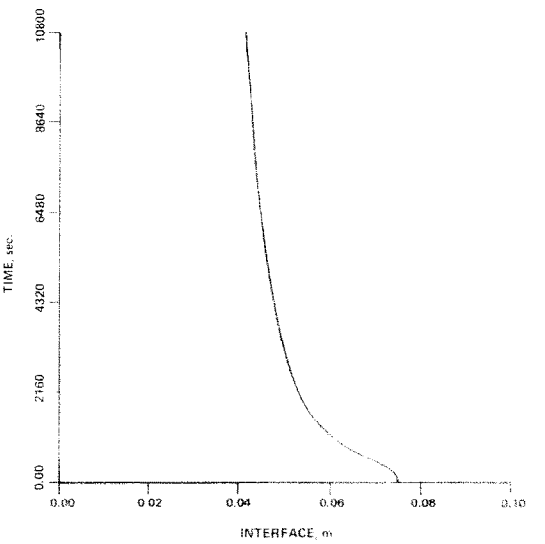

FIG. 3. Plot of the interface position.

this range. Once s_n is known the temperature and concentration are obtained by integrating

$$r'_{-} = \left(\frac{\hat{c}\rho}{\Delta t}\right)_{-} [R_{-}(x)r_{-} + w_{-}(x) - u_{n-1}(x)] \quad (17)$$

$$r'_{+} = \left(\frac{1}{\Delta t}\right)[S_{+}(x)r_{+} + z_{+}(x) - c_{n-1}(x)] \quad (18)$$

subject to the computed fluxes on the phase front s_n, and by substituting these functions into equations (9) and (10) (see, again, [4]).

The numerical solution of these equations can proceed as follows. We assume the solution is given at t_{n-1}. A grid is defined on the interval $[0, L]$ and a time step Δt is chosen. Then $R_{\pm}$ and $S_{\pm}$ are found at each grid point. If the physical parameters are constant then R_{-} and S_{+} are available in closed form because the equation

$$Y' = a - bY^2, \quad Y(X) = 0$$

has the solution

$$Y(x) = \sqrt{(a/b)}\tanh\sqrt{(ab)}(x - X).$$

Note that $R_{\pm}$ and $S_{\pm}$ need not be recalculated at each time step unless Δt is changed. Next w_{-} and z_{-} are integrated numerically from $x = L$ to $\hat{x} < s(t_{n-1})$ where $\hat{x}$ is chosen so small that the new interface can be expected to lie to the right of $\hat{x}$. Then w_{+} and z_{+} are integrated from $x = 0$ to $\hat{x}$ where $\hat{x}$ is chosen so large that s_n is expected to lie to the left of $\hat{x}$. On the interval $(\hat{x}, \hat{x})$ the equation $\phi(x) = 0$ is solved for s_n. Finally, the equations (17) and (18) are integrated and the results substituted into (9) and (10).

The current computer code is based on a fixed but not necessarily uniform grid and on closed form solutions for $R_{\pm}$ and $S_{\pm}$. The equations (13) and (17) are integrated with the trapezoidal rule; however, the equations (14) and (18) are extremely stiff ($1/\Delta t\, S_{-}(x) \sim 10^5$) so that an implicit Euler method appears more advantageous than the higher order trapezoidal rule. The root of $\phi(x) = 0$ is determined by finding two adjacent mesh points x_{i-1}, x_i between which ϕ changes sign, and by obtaining s_n as the zero of the quadratic interpolant to ϕ at x_{i-2}, x_{i-1} and x_i.

3. A NUMERICAL EXAMPLE

The applicability of the method is shown by computing the solidification process for a typical metal alloy. The physical constants are $k_{+} = 10$, $k_{-} = 20$, $\hat{c}_{+} = 400$, $\hat{c}_{-} = 600$, $\rho_{+} = \rho_{-} = 6 \times 10^3$, $\lambda = 250$, $D_{+} = 10^{-9}$, $D_{-} = 10^{-11}$. It may be noted that the thermal and mass diffusivities differ by five to seven orders of magnitude. The phase is shown in Fig. 1. Initial conditions are $u_0(x) = 1100$, $c_0(x) = 0.7$ in the liquid, $c_0(x) = 0.3$ in the solid, $s_0 = 0.075$, $L = 0.1$. The boundary conditions are $\alpha_{+}(t) = 1100$, $\alpha_{-}(t) = 1000$, $\beta_{+}(t) = 0.7$, $\beta_{-}(t) = 0.3$, $t > 0$. The temperature is discontinuous at $t = 0$ at the solid end while the initial interface concentration is compatible with the phase diagram.

Figures 2, 3 and 4 show some computed results for a 10 cm slab. The space mesh is 0.02 cm for the first 4 cm and 0.005 cm for the remaining 6 cm. Time steps are $\Delta t = 2$ s for $t \in (0, 600]$,

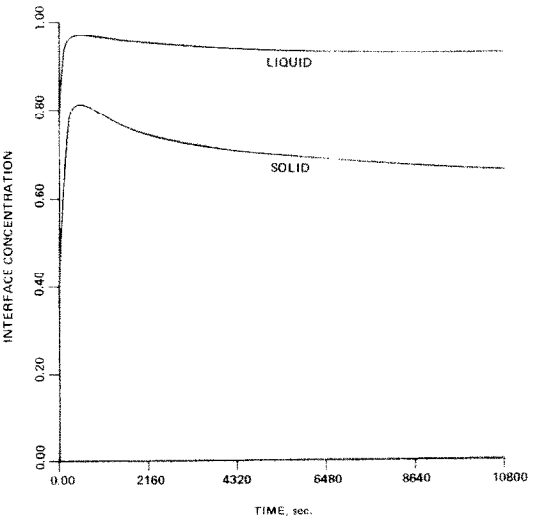

FIG. 4. Plot of the interface concentrations as a function of time.

$\Delta t = 5$ s for $t \in (600, 1200]$, $\Delta t = 10$ s for $t \in (1200, 1800]$, $\Delta t = 30$ s for $t \in (1800, 3600]$, $\Delta t = 60$ s for $t \in (3600, 7200]$ and $\Delta t = 120$ s for $t \in (7200, 10\,800]$. A fine grid appears desirable, at least near the interface, because of extremely steep concentration gradients as shown in Fig. 2. The solid lines in this illustration indicate the computed concentrations of one constituent in the liquid and solid after 10 min and 3 h. There is a sharp increase in the concentration of both phases near the interface, and little diffusion takes place out of the newly solidified metal into the rest of the solid. The temperature profile throughout the slab is already in its final steady-state at $t = 10$ min and is not shown. As in [3] we also indicate the maximum permissible concentrations corresponding to the computed temperature profiles. They are the liquid and solid concentrations obtained for the given temperature from the phase diagram. Since the permitted liquid concentration lies above the actual concentration the liquid is constitutionally supercooled. Similarly, the solid is superheated near the interface after 3 h. Figure 3 shows the phase front and Fig. 4 gives the interface concentrations as a function of time. The interface temperature (not shown) decreases for about 8 min and then begins to climb again. These results are qualitatively correct (see, e.g. [1], p. 150). Quantitatively, they are very stable with respect to changes in the space mesh but show some change with Δt, for example, $s(600) = 0.0716$ for $\Delta t = 30$ s, $s(600) = 0.0687$ for $\Delta t = 5$ s, $s(600) = 0.0677$ for $\Delta t = 3$ s, $s(600) = 0.06705$ for $\Delta t = 2$ s. This behavior indicates that a production computer code for the above problem should be based on a second order time discretization. On the other hand, because the slab is thin, the temperature change is rapid and the supercooling is substantial this application appears to be very severe. Yet the method even in its relatively simple implementation can effectively and quickly solve this one-dimensional solidification problem. Finally, the method is readily applicable to much more complicated one-dimensional problems. Whether it can be used in conjunction with locally one-dimensional methods for multi-dimensional problems remains to be examined.

Acknowledgement—This work was supported in part by the U.S. Army Research Office under Contract DAAG29–79–C–0145.

REFERENCES

1. B. Chalmers, *Principles of Solidification*. Wiley, New York (1964).
2. A. B. Crowley and J. R. Ockendon, On the numerical solution of an alloy solidification problem, *Int. J. Heat Mass Transfer* **22**, 941–948 (1979).
3. B. Lewis, *Nucleation and Growth Theory, in Crystal Growth* (edited by B. R. Pamplin. Pergamon Press, Oxford (1975).
4. G. M. Meyer, *Initial Value Methods for Boundary Value Problems*. Academic Press, New York (1973).